

# Estimates of Constrained Coded Modulation Capacity for Optical Networks

Tobias Fehenberger<sup>1,\*</sup>, Felix Kristl<sup>1</sup>, Carsten Behrens<sup>2</sup>, Armin Ehrhardt<sup>3</sup>, Andreas Gladisch<sup>2</sup>, and Norbert Hanik<sup>1</sup>

<sup>1</sup>Institute for Communications Engineering, Technische Universität München, 80333 München

<sup>2</sup>Telekom Innovation Laboratories, Winterfeldtstr. 21, 10781 Berlin

<sup>3</sup>Deutsche Telekom Technik GmbH, FMED 24, Winterfeldtstr. 21, 10781 Berlin

\*Email: tobias.fehenberger@tum.de

## ABSTRACT

For advanced FEC schemes with soft-decision decoding, the mutual information (MI) between sent and received symbols is the natural figure of merit at the decoder input. In this work, the transmission of signals modulated with rectangular quadrature amplitude modulation (QAM) of order 16, 64, and 256 is simulated over three different fiber links that are typical representatives of metro-area networks used by Deutsche Telekom. At the receiver, the MI between sent and received symbols is estimated using histograms for which the correct bin number is determined in a reliable way. As MI is the constrained capacity, the channel capacity of an optical communication system including all components at transmitter and receiver is found. From the capacity we can derive the maximum spectral efficiency and the maximum data rate over the entire available spectrum for a fixed transmitter, link, and receiver design. For an average metro-area network link, more than 26 Tbit/s at a 50 GHz spacing are possible over the entire C-band. By decreasing the spacing to be close to the Nyquist rate, a dual-polarization spectral efficiency of 10.8 bit/s/Hz is possible, which increases the maximum total data rate per fiber to an astonishing 43.2 Tbit/s.

## I. INTRODUCTION

Driven by broadband services such as video streaming, the demand for higher data rates in optical networks has been growing for years. While the operators wish to use their currently deployed fibers, new spatially multiplexed fibers with more than one mode or core per fiber are often considered the most promising solution to the anticipated capacity crunch [1], [2]. An interesting open question for operators is what the maximum throughput over the deployed links is and at which point an upgrade to new types of fiber becomes inevitable.

An alternative to spatially-multiplexed fibers is to use the current standard single-mode fibers and higher-order modulation schemes such QAM with 16 and more constellation points. As the noise susceptibility of these formats in general increases with modulation order, stronger forward error correction (FEC) must be used. One major step in this direction are coding schemes whose decoder operates with soft-input instead of hard input. For these advanced coding schemes and their decoders, the bit error ratio (BER) at the decoder input, denoted  $\text{BER}_{\text{in}}$ , has no relation to the BER after decoding, denoted  $\text{BER}_{\text{out}}$ . This is because the BER does not represent the reliability of a decision, which is fundamental for soft-input decoders. Hence, it makes no sense to continue using the BER or the  $Q^2$  factor as a function of  $\text{BER}_{\text{in}}$  as figure of merit. Instead, MI is a natural figure of merit in the context of soft-decision decoding [3]. Recent experimental work [4] and simulations [5] have also shown that MI is robust and reliable for determining  $\text{BER}_{\text{out}}$  without actually doing the decoding.

Apart from being a suitable figure of merit, MI is the rate of reliable communication. This allows us to determine the maximum constrained channel capacity and thus the maxi-

imum transmission rate of an optical fiber system. We apply this method to an optical transmission network to determine the modulation format that offers the best trade-off between complexity and performance.

This paper is organized as follows. Section II reviews aspects of information-theory that are required later in this work. In Section III, a method to reliably estimate MI is presented. The simulation setup of link layouts typical for a metro-area network of Deutsche Telekom is given in Section IV. For these links, the constrained capacity results are discussed in Section V. Section VI concludes this work.

## II. INFORMATION THEORY

### A. Capacity and Mutual Information

Fundamental work of information theory [6] tells us that capacity is the ultimate performance limit of communication. Particularly, the converse of Shannon's channel coding theorem states that if the rate of transmission is larger than the channel capacity, an arbitrarily small BER after decoding cannot be reached. The forward version of this theorem implies that there exist codes with block length approaching infinity that allow an arbitrarily small bit error rate after decoding to be reached if the rate of transmission is smaller than capacity. Unfortunately, Shannon's proof of this theorem was not constructive as no method to construct such codes was presented. Only recently, polar codes [7] and convolutional low-density parity-check (LDPC) codes [8] have shown to asymptotically achieve this performance for an additive white Gaussian noise (AWGN) channel.

For a formal definition of capacity, consider a memoryless channel whose input  $X$  and output  $Y$  are discrete random variables. In this work, we consider the discrete case only as

it is most relevant for a practical application with sampling at transmitter and receiver. The capacity  $C$  is the maximum MI over all possible input distributions  $p_X$ ,

$$C = \max_{p_X} I(X; Y). \quad (1)$$

In practical scenarios, discrete modulation with a finite number of modulation symbols is used. If the modulation scheme is fixed, the maximization over  $p_X$  is dropped, resulting in the so-called *constrained capacity*,

$$C^* = I(X; Y). \quad (2)$$

In the analysis carried out later,  $X$  and  $Y$  represent symbol input and output, and  $C^*$  is the constrained coded modulation capacity. For simplicity, we refer to it as constrained capacity for the rest of this work.

If we wish to find the capacity of any channel for a certain modulation scheme, the MI is to be determined. It is formally defined as (see e.g. [9])

$$I(X; Y) = \sum_{m=1}^M \sum_{y \in \mathcal{Y}} p_X(x) p_{Y|X}(y|x_m) \log_2 \left[ \frac{p_{Y|X}(y|x_m)}{p_Y(y)} \right], \quad (3)$$

with  $p_X(x)$  being the input distribution,  $p_Y(y)$  the output distribution, and  $p_{Y|X}(y|x_m)$  the conditional distribution of the output given the input.  $M$  denotes the modulation order. According to (3), estimating MI is essentially a task of estimating the distribution of symbols after being transmitted over an unknown channel. In the next section, we present a method to reliably perform this estimation.

### III. HISTOGRAMS TO ESTIMATE MUTUAL INFORMATION

#### A. Histograms

We know from the previous section that the probability mass functions  $p_Y(y)$  and  $p_{Y|X}(y|x_m)$  are to be estimated. A common way to do this is to use histograms. Given a sequence of symbols drawn according to some unknown distribution, histograms operate by dividing the entire range of symbols into intervals of a certain width. The number of symbols falling into each so-called bin represents the probability of occurrence for this range of symbols. If the symbols are complex, a two-dimensional histogram must be used. In this work, the number of bins of one dimension is independent of the other one and the width of a bin is constant along each dimension.

The bin number is a crucial parameter for the accuracy of estimating distributions. This is illustrated in Fig. 1 for 10000 quadrature phase-shift keying (QPSK) symbols transmitted over an circular symmetric AWGN channel with varying signal-to-noise ratio (SNR). The MI estimated with histograms of different bin sizes per dimension is compared to the numerically calculated constrained capacity. According to (2), they should be identical. For too few bins, however, the true structure of the probability density function can no longer be represented by the histogram and the estimation is too coarse to yield reliable results. If the bin number is too high, MI is overestimated because of the discrete nature of simulations and processing. Since simulations must be carried out with a limited amount of bits due to computational performance and

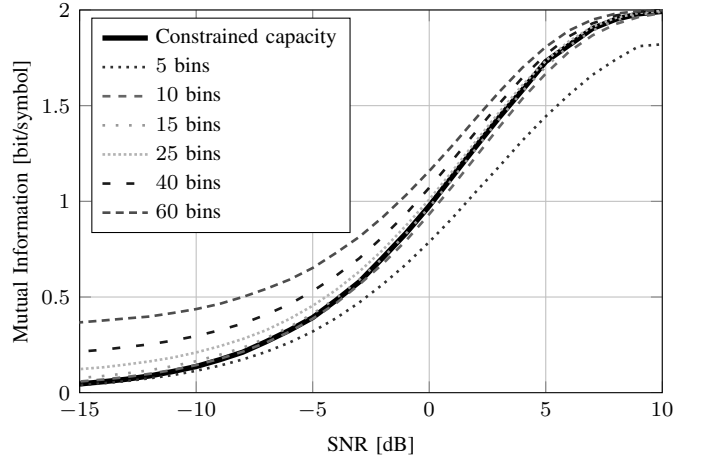


Fig. 1. Comparison of MI for different histogram bin sizes per dimension with the constrained capacity of QPSK over an AWGN channel.

real life requirements, some bins - especially those in the low probability areas - will be completely empty if the total number of bins is high. This means that both  $p_{Y|X}(y|x_m)$  and  $p_Y(y)$  in (3) are zero. For these empty bins, the calculation of the MI yields  $\log_2 \frac{0}{0}$ . As this is not defined, the contribution of these empty bins to the MI must be considered zero while their true contribution would actually be a small negative value. The more empty bins exist, the more negative summands are falsely excluded and the higher the overestimation of MI is. Additionally, the optimal bin size depends also on the amount of symbols considered per histogram operation. This becomes clear when assuming that by increasing the number of symbols and keeping all other parameters unchanged, there are fewer empty bins and the correct bin number for a reliable distribution estimate must be increased.

In order to deal with the outlined dependencies of the histogram output, we present in the following a method to find the correct number of bins per dimension.

#### B. Correct number of bins

A recent method [10] determines the correct number of bins based solely on data and not on the underlying probability density function. The idea is to minimize the error between the density model obtained by the method and the unknown true density. This distinguishes this method from many other techniques for distribution estimation and provides it with generality. Due to space constraints, only the key equation of [10] for a two-dimensional data set is given. The correct pair of bin numbers  $\{\hat{M}_x, \hat{M}_y\}$  is

$$\begin{aligned} \{\hat{M}_x, \hat{M}_y\} = \arg \max_{M_x, M_y} & \left\{ N \log M_x M_y + \log \Gamma \left( \frac{M_x M_y}{2} \right) + \right. \\ & - M_x M_y \log \Gamma \left( \frac{1}{2} \right) - \log \Gamma \left( N + \frac{M_x M_y}{2} \right) + \\ & \left. + \sum_{k=1}^{M_x} \sum_{l=1}^{M_y} \log \Gamma \left( n_{k,l} + \frac{1}{2} \right) + K \right\}. \quad (4) \end{aligned}$$

For (4),  $N$  data points and  $M_x$  histogram bins with equal width along the in-phase dimension and  $M_y$  bins for the

quadrature are assumed.  $\Gamma$  denotes the gamma function,  $\Gamma(x) = \int_0^\infty e^{-t} t^{x-1} dt$ ,  $K$  is an implicit proportionality constant, and  $n_{k,l}$  is the number of samples falling into the  $k^{\text{th}}$  bin of the in-phase and  $l^{\text{th}}$  bin of the quadrature if a two-dimensional histogram with  $\{M_x, M_y\}$  bins is performed. The maximization problem of (4) is solved with a brute-force approach by jointly probing a certain range of  $\{M_x, M_y\}$  and choosing the one that results in the largest function value. [10] as well as our simulations suggest that the largest bin number to be tested can be limited to a reasonably large number as too many bins result in overestimating MI and thus decrease the function to be maximized in (4). In this work an upper limit of 100 bins per dimension is used when solving the maximization problem.

### C. Comparison with AWGN capacity

We compare the MI estimate according to (4) with the actual constrained capacity of QPSK. As the capacity of an optical fiber is not known, we use a circular symmetric AWGN channel as reference. It has been shown in simulations [11] and experiments [12] that the noise distribution at the receiver after transmission over an optical fiber with high baud rate is approximately Gaussian. For the Gaussian AWGN channel, the channel capacity can be calculated numerically [13]. The MI and the constrained channel capacity over SNR are shown in Fig. 2 for QPSK symbols transmitted over a circular symmetric AWGN channel. 10000 symbols are considered per histogram operation. A good match of the MI estimate and constrained capacity is visible with the two curves being hardly distinguishable at high SNRs. Further simulations have shown that this excellent match is also present for a different number of symbols per histogram operation and rectangular QAM of order 16 and 64. For 256-QAM, the method starts to show some instabilities that are further discussed in Section V. For the AWGN channel, which is a widely accepted approximation to the optical fiber channel, the presented method to estimate MI shows great accuracy over the entire SNR range. It is thereby justified to use this method to determine the constrained capacity of an optical communication system. In the following, the analysis is applied via simulations to a fiber network.

## IV. SIMULATION SETUP

We determine the constrained capacity for 16-QAM, 64-QAM, 256-QAM and three different link layouts in simulations. The links are taken from Deutsche Telekom and are representatives of the shortest and longest link in the metro-area network as well as an average link. The layout and fiber parameters are given in Tables I and II. Further simulation parameters can be found in Table III.

Each span consists of single-mode fiber (SMF) of a certain length, an Erbium-doped fiber amplifier (EDFA), a dispersion-compensating fiber (DCF) and another EDFA. Five times along the link, an EDFA-DCF-EDFA block is expanded by a (reconfigurable) optical add-drop multiplexer ((R)OADM). These devices are modeled as ideal bandpass filters that remove all wavelength-division multiplexed (WDM) channels

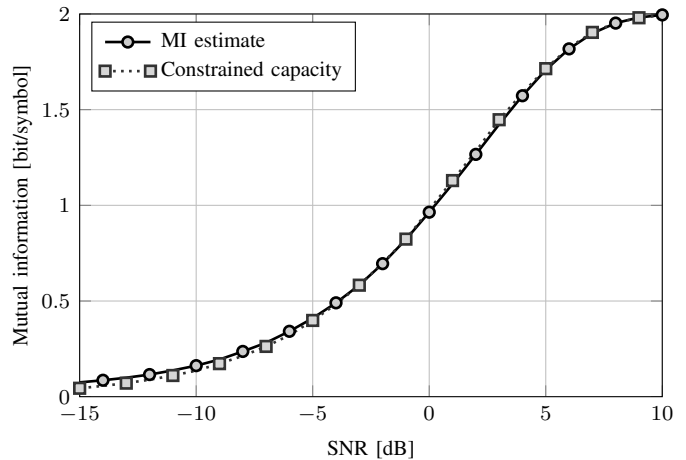


Fig. 2. Comparison of the constrained capacity of QPSK with the MI estimate over an AWGN channel. 10000 symbols are simulated.

except for the center one and randomly add new ones such that the number of co-propagating channels equals the original number. The propagation of the optical signal over the fiber is simulated by solving the nonlinear Schrödinger equation numerically using the split-step Fourier method (SSFM) [14] with 32 samples per second (SpS). The DCFs compensate for about 90% of the SMF chromatic dispersion (CD).

At the transmitter, a bit sequence of length  $2^{18}$  is created, mapped onto either 16-QAM, 64-QAM, or 256-QAM symbols and transferred into the optical domain. A root-raised cosine (RRC) filter is used for pulse shaping. The baud rate is 28 Gbaud. 9 co-propagating channels spaced at 50 GHz are launched into the fiber. At the receiver, an ideal coherent front-end with ideal optical band-pass filtering transforms the WDM channel of interest into the digital domain where any residual CD not compensated by DCFs is removed digitally. Ultimately, MI is calculated as outlined in Section III.

Both transmitter and receiver are kept relatively simple as we wish to determine the fiber capacity without having vendor-dependent component imperfections or the choice for or against certain digital signal processing (DSP) algorithms influence the results. Both digital-to-analog converter (DAC) and analog-to-digital converter (ADC) are ideal, as well as the Mach-Zehnder modulator (MZM). The lasers at the transmitter and receiver have zero linewidth and no frequency offset, which makes carrier phase recovery (CPR) redundant. Without any polarization-mode dispersion (PMD) on the fiber and by fulfilling the first Nyquist criterion, equalization is not required either. Applying a FEC is not necessary because the analysis via MI inherently assumes an ideal coding scheme.

TABLE I  
PARAMETERS FOR THE SHORT, AVERAGE, AND LONG LINK

Path type	SMF length	# spans	# EDFAs	# (R)OADMs
Long link	933 km	15	38	5
Average link	355 km	8	20	5
Short link	152 km	6	16	5

TABLE II  
FIBER PARAMETERS

Parameter	SMF	DCF
$\alpha$ [dB/km]	0.25	0.5
$D$ [ps/km/nm]	17	-100
$\gamma$ [1/W/km]	1.3	0
PMD	0	
EDFA noise figure	5 dB	
(R)OADM insertion loss	10 dB	

TABLE III  
SIMULATION PARAMETERS

Bits per pol.	$2^{18}$
Modulation format	{16, 64, 256}-QAM
DAC	ideal
MZM	ideal
Pulse-Shaping	RRC
RRC Roll-off	0.05
Samples per symbol	32
Baud rate per pol.	28 GBaud
WDM channels	9
Default WDM spacing	50 GHz
Channel of interest	center
Optical filter	ideal band-pass
Coherent receiver	ideal
ADC	ideal
CD compensation	ideal

## V. SIMULATION RESULTS

We apply the method discussed in Section III to the setup outlined in Section V. First, we determine the constrained channel capacity and hence the total maximum data rate of the three links. In the second set of simulations, we use MI as a relative figure of merit to quantify the impact of two different approaches to compensate CD as well as the impact of the WDM spacing on the capacity. In Figs. 3, 4, and 5, MI over launch power per channel is depicted for the short, average and long link, respectively. The launch power is increased in increments of 1 dBm for all simulations. For the three links, MI follows the typical behavior of a nonlinear fiber system. In the low-power region, the performance is limited by noise from the optical amplifiers. By increasing the launch power per channel, the signal quality increases until a maximum MI is reached at an optimum power level of about  $-2$  dBm. When further increasing the power, the system is driven into the nonlinear regime and MI is decreasing. In Fig. 3, the MI of 16-QAM and 64-QAM exhibits a clear plateau over a broad range of launch powers because the limit of these modulation formats is  $\log_2 M$  where  $M$  is the modulation order. In the case of 16-QAM, a maximum of  $\log_2 16 = 4$  bit/symbol can be transmitted regardless of the link quality. MI tells us that in the considered scenario, 256-QAM is the preferred modulation format because it achieves almost 7.5 bit/symbol per polarization with ideal FEC. In Fig. 4, the MI of the three modulation formats is depicted for the average link. The behavior is very similar compared to the short link. Having a longer link and thus more nonlinearities and more noise from the EDFAs, only 16-QAM reaches its plateau at 4 bit/symbol. 64-QAM and 256-QAM have

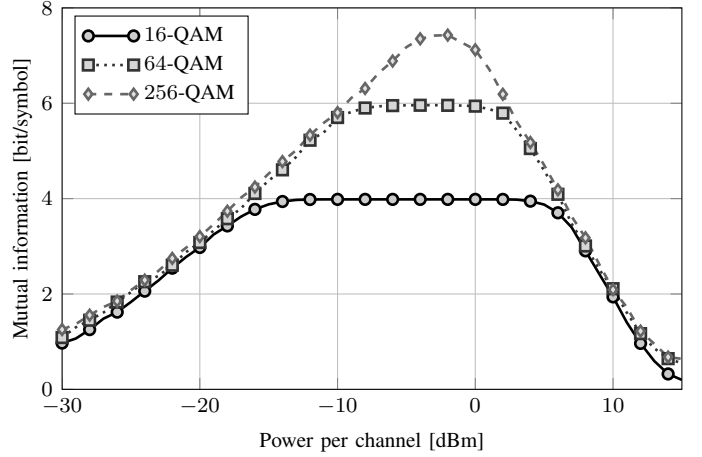


Fig. 3. MI over launch power in increments of 1 dBm for 16-QAM, 64-QAM, 256-QAM for the short link.

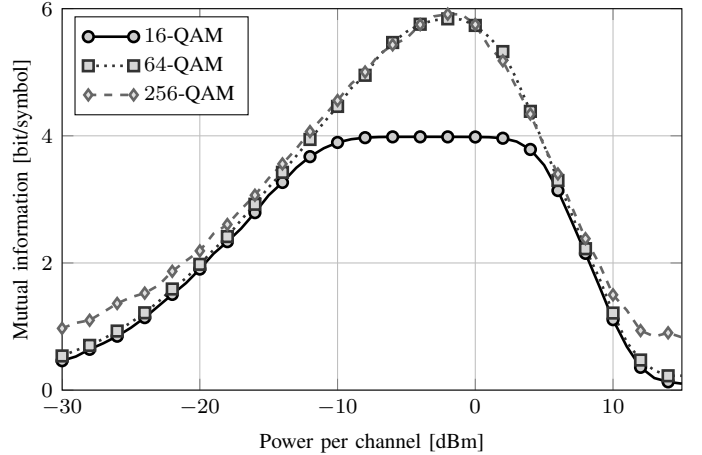


Fig. 4. MI over launch power in increments of 1 dBm for 16-QAM, 64-QAM, 256-QAM for the average link.

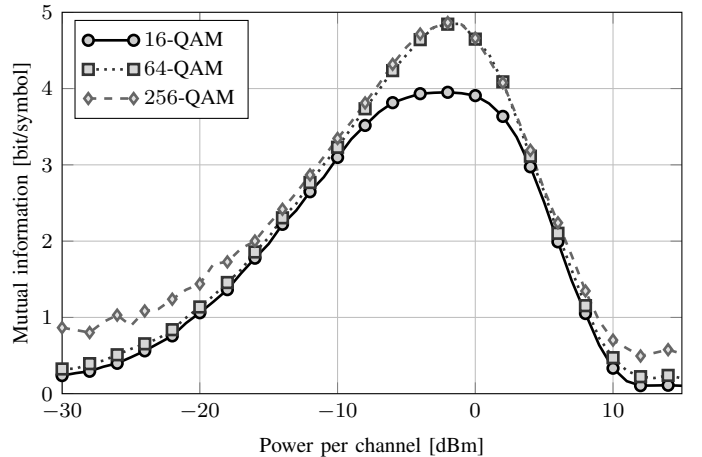


Fig. 5. MI over launch power in increments of 1 dBm for 16-QAM, 64-QAM, 256-QAM for the long link.

approximately the same MI at the optimum launch power. This means that their capacity is identical, yet 256-QAM imposes even higher requirements on components and DSP algorithms. We conclude that for the average link, 64-QAM offers the best trade-off between complexity and performance and is the preferred modulation format with 5.8 bit/symbol. The same line of argument holds for the longest link shown in Fig. 5. Note that the simulation results of the average and long link suggest that 256-QAM outperforms the two other modulation formats in the extremely high and low power regime. Actually, this is not true because the difference between the modulation schemes is expected to be very small for very high noise levels, see e.g Fig. 3. We attribute this deviation to an instability of the distribution estimation method that starts to appear when the amount of distortion and the modulation order are both very high. In this case, the constellation diagram at the receiver is heavily distorted having virtually no resemblance to the sent constellation. When the noise power decreases and/or the modulation order becomes smaller, the method is stable, as it is the case for 16-QAM and 64-QAM at all noise levels and 256-QAM at moderate and low noise levels.

For the rest of this work, namely the simulation results shown from Fig. 6 up to and including Fig. 10, only the average link is considered.

Fig. 6 shows the the total achievable transmission rate over both polarizations for the average link if the entire C-band is occupied with 80 WDM channels spaced at 50 GHz, each carrying  $28 \cdot 10^9$  QAM symbols per second. 9 WDM channels are simulated as the impact of channels spaced further apart is negligible [15]. A maximum net data rate of 26 Tbit/s per fiber is possible with an ideal transmitter and receiver over the average link even if the available bandwidth is not used as efficiently as it could be if the system operated at the Nyquist limit.

In Fig. 7, the maximum coding rate is depicted. The rate is calculated in a straightforward fashion by dividing the MIs from Fig. 4 for each modulation format by the respective  $\log_2 M$ . The rate of Fig. 7 is the maximum rate that can be used if an arbitrarily small BER is to be achieved. This follows directly from Shannon's channel coding theorem. Conversely, any coding scheme with a larger rate will definitely result in a  $\text{BER}_{\text{out}}$  that is not arbitrarily small and hence too high for the requirements in optical communications. As  $(1/\text{rate}) - 1$  specifies the coding overhead that the assumed ideal FEC must have, about 35% overhead is required for 256-QAM, 3% overhead for 64-QAM and less than a percent for 16-QAM. Note that this is a limit for an ideal code. Any non-ideal FEC will require a larger overhead.

Fig. 8 shows the impact of different CD compensation methods for the average link and 64-QAM. All previous results are created with DCFs without nonlinear interference (NLI). When a realistic  $\gamma$  of  $5.8 \text{ W}^{-1} \text{ km}^{-1}$  is simulated instead, the maximum MI drops by 0.3 bit/symbol. The optimal launch is also decreased as more nonlinear fiber leads to a stronger impact of nonlinearities. When the compensation is done fully digital at the receiver and each DCF as well as the following EDFA is removed, a maximum MI gain of 0.4 bit/symbol compared to the case with NLI can be seen. In comparison to

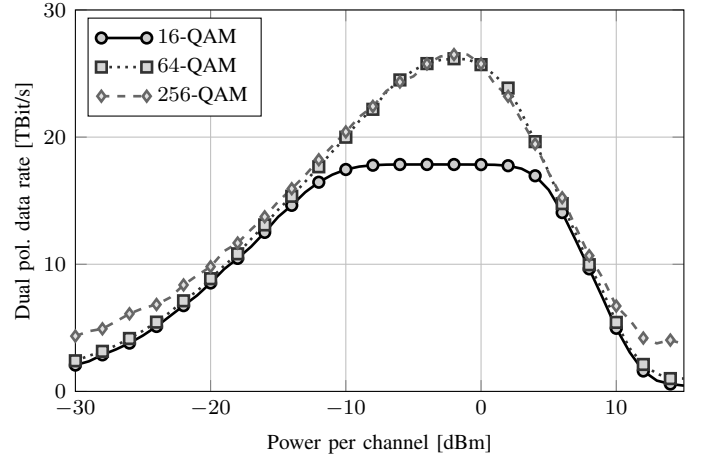


Fig. 6. Total possible transmission rate achievable with 16-QAM, 64-QAM, 256-QAM for the average link.

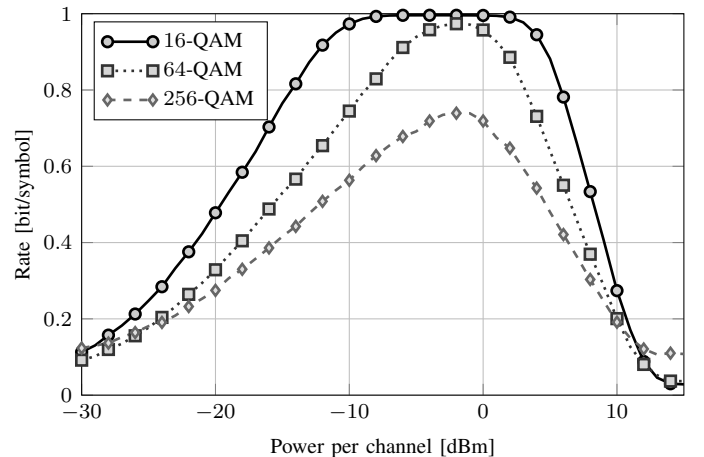


Fig. 7. Rate over launch power for 16-QAM, 64-QAM, 256-QAM for the average link.

the idealized DCF without NLI, the maximum MI is increased by 0.1 bit/symbol. Further simulations suggest that it is not the omitted EDFAs that lead to this difference but the fact that the nonlinearities add up coherently during propagation when in-line compensation is performed.

Fig. 9 shows the MI over launch power for the average link, 64-QAM, and WDM spacings from 25 GHz to 50 GHz in increments of 5 GHz. The signal with a symbol rate of 28 GBaud and an RRC filter with 0.05 roll-off occupies  $28 \cdot 1.05 = 29.4$  GHz bandwidth. For all WDM spacings larger than this value, the MI in the linear regime does not change. In the nonlinear regime, the decreased channel spacing leads to decreased phase mismatch and thus, stronger impact of NLI, which explains why MI decreases with decreasing channel spacing. For channel spacing of 25 GHz, the WDM channels overlap. As this interference is essentially additional noise, the performance is heavily degraded compared to other spacings. Note that the number of channels is kept constant at 9. The total simulated bandwidth of the system is thus smaller for a more densely spaced WDM grid. Although the nonlinear impact of a channel decreases with spacing, the performance of the smaller spacings might be slightly overestimated compared to the reference 50 GHz.

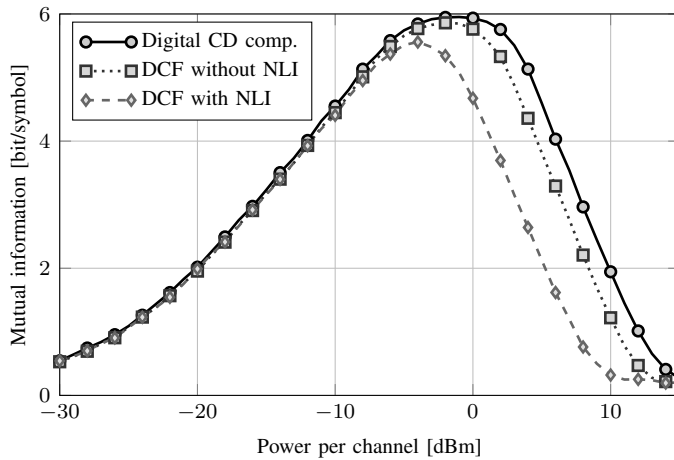


Fig. 8. Different approaches to compensate CD for 64-QAM and the average link.

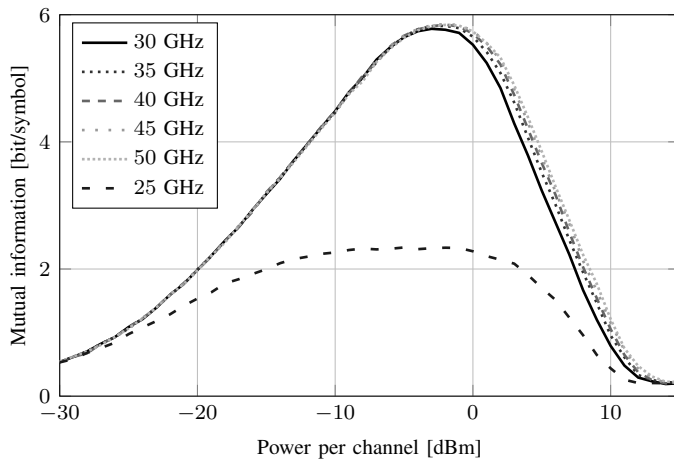


Fig. 9. Mutual information of various WDM grid spacings for 64-QAM and the average link.

Based on the curves of Fig. 9, the dual-polarization (DP) spectral efficiency (SE) for all simulated WDM spacings and 64-QAM over the average link is depicted in Fig. 10. The spacing that is closest to the Nyquist rate shows the best performance with a dual-polarization net SE of about 10.8 bit/s/Hz. This corresponds to 43.2 Tbit/s if the entire C-band is used.

## VI. CONCLUSION

We have presented a histogram-based method to reliably estimate the MI and hence the constrained coded modulation capacity. The accuracy of this method is shown in comparison to the numerically calculated constrained capacity of QPSK over an AWGN channel. Instabilities that are irrelevant in practical applications are found for 256-QAM at very high noise. We estimate the MI of three metro-area network links and for three different QAM schemes via simulations. From this analysis, the modulation format that offers the best trade-off between performance and complexity is determined. For an average metro-area link, 64-QAM is found to be this optimum, reaching 5.8 bit/symbol. A total data rate of 26 Tbit/s for a 50 GHz WDM spacing and more than 43 Tbit/s for a 30 GHz

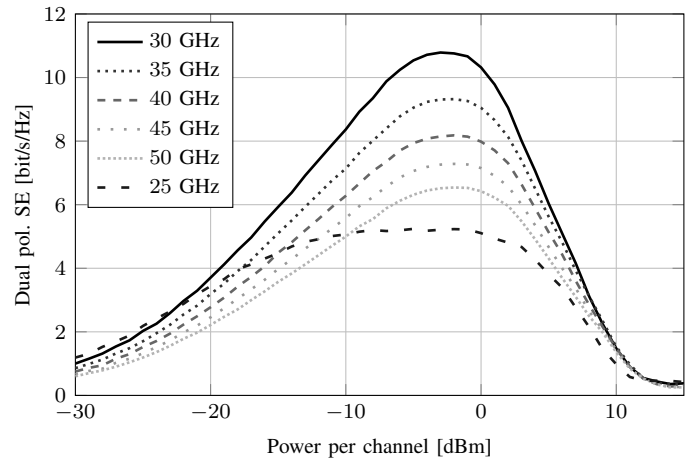


Fig. 10. Dual-polarization SE for various WDM grid spacings, 64-QAM and the average link.

spacing are possible in this case if ideal FEC is used. These impressive data rates are achieved for an idealized transmitter and receiver. An interesting future research direction is to quantify the impact of component imperfections and DSP algorithms. Also, changing the link layout without deploying new fibers, e.g. by varying the EDFA spacing or the dispersion map might further increase the possible data rate.

## REFERENCES

- [1] A. Chraplyvy, "The coming capacity crunch," in *Proc. European Conference on Optical Communication (ECOC)*, Paper Mo.1.0.2, 2009.
- [2] P. J. Winzer, "Spatial multiplexing: The next frontier in network capacity scaling," in *Proc. European Conference on Optical Communication (ECOC)*, Paper We.1.D.1, 2013.
- [3] M. Tuechler, S. ten Brink, and J. Hagenauer, "Measures for tracing convergence of iterative decoding algorithms," in *Proc. 4th Int. ITG Conf. Source and Channel Coding*, 2002.
- [4] A. Leven, F. Vacondio, L. Schmalen, S. ten Brink, and W. Idler, "Estimation of soft FEC performance in optical transmission experiments," *IEEE Photon. Technol. Lett.*, vol. 23, no. 20, pp. 1547–1549, Oct. 2011.
- [5] T. Fehenberger and N. Hanik, "Information quality (IQ) factor as soft-decision decoding threshold for optical communications," in *Proc. European Conference on Optical Communication (ECOC)*, P.4.12, 2013.
- [6] C. E. Shannon, "A mathematical theory of communication," *Bell Labs Techn. J.*, vol. 27, pp. 379–423 and 623–656, Jul. 1948.
- [7] E. Arkan, "Channel polarization: A method for constructing capacity-achieving codes for symmetric binary-input memoryless channels," *IEEE Trans. Inf. Theory*, vol. 55, no. 7, pp. 3051–3073, Jul. 2009.
- [8] S. Kudekar, T. Richardson, and R. L. Urbanke, "Spatially coupled ensembles universally achieve capacity under belief propagation," *IEEE Trans. Inf. Theory*, vol. 59, no. 12, pp. 7761–7813, Dec. 2013.
- [9] L. Hanzo, S. X. Ng, T. Keller, and W. Webb, *Quadrature Amplitude Modulation*, 2nd ed. West Sussex, UK: IEEE Press, 2004.
- [10] K. Knuth, "Optimal data-based binning for histograms," *arXiv:physics/0605197v2*, Sep. 2013.
- [11] S. Kilmurray, T. Fehenberger, P. Bayvel, and R. Killey, "Comparison of the nonlinear transmission performance of quasi-Nyquist WDM and reduced guard interval OFDM," *Opt. Express*, vol. 20, no. 4, pp. 4198–4205, Feb. 2012.
- [12] P. Poggiolini, "The GN model of non-linear propagation in uncompensated coherent optical systems," *J. Lightw. Technol.*, vol. 30, no. 24, pp. 3857–3879, Dec. 2012.
- [13] G. Ungerboeck, "Channel coding with multilevel/phase signals," *IEEE Trans. Inf. Theory*, vol. IT-28, no. 1, pp. 55–67, Jan. 1982.
- [14] O. Sinkin, R. Holzlohner, J. Zweck, and C. Menyuk, "Optimization of the split-step Fourier method in modeling optical-fiber communications systems," *J. Lightw. Technol.*, vol. 21, no. 1, pp. 61–68, Jan. 2003.
- [15] R.-J. Essiambre, G. Kramer, P. J. Winzer, G. J. Foschini, and B. Goebel, "Capacity limits of optical fiber networks," *J. Lightw. Technol.*, vol. 28, no. 4, pp. 662–701, Feb. 2010.